AGE (2014) 36:9691
DOI 10.1007/s11357-014-9691-7

Structural investigation of donor age effect on human bone marrow mesenchymal stem cells: FTIR spectroscopy and imaging

Ceren Aksoy · Fatima Aerts Kaya · Bülent Barış Kuşkonmaz · Duygu Uçkan · Feride Severcan

Received: 28 December 2013 / Accepted: 17 July 2014 / Published online: 1 August 2014
© American Aging Association 2014

Abstract Stem cell studies hold enormous potential for development of new therapies for tissue regeneration and repair. Bone marrow mesenchymal stem cells (BM-MSCs) can differentiate into a variety of non-hematopoietic tissues and contribute maintenance of healthy hematopoiesis by providing supportive cellular microenvironment into BM. Here, we investigated age-related differences in BM-MSCs by using attenuated total reflection Fourier transform infrared (ATR-FTIR) spectroscopy and FTIR imaging together with hierarchical clustering as a novel methods to clarify global alterations in the structure and function of macromolecules in characterized BM-MSCs of different aged donors. The results may contribute to identification of age-related new molecular marker(s) to determine the effects of donor age on MSCs. The spectral results reflected that there were significant increases in the concentration of saturated lipids, proteins, glycogen, and nucleic acids in children and adolescent group BM-MSCs when compared to the infants and early and mid adults. The concentration of mentioned macromolecules in adult (early and mid) BM-MSCs were significantly lower than the concentrations in the children and adolescents. These results were attributed to the increase in the proliferation activity in younger BM-MSCs. The distribution of macromolecules into the cells was shown as in the form of chemical maps by FTIR imaging, and the results are in agreement with the ATR-FTIR spectroscopy results. The cellular activity degree was determined by the thiazolyl blue tetrazolium bromide (MTT) proliferation assay to support ATR-FTIR spectroscopy results. BM-MSCs of five different age groups were discriminated by making the hierarchical cluster analysis where the spectral data according to alterations in structure and composition of macromolecules were considered.

Keywords ATR-FTIR spectroscopy · FTIR imaging · Bone marrow mesenchymal stem cells · Stem cell aging · Donor age effect

C. Aksoy
Department of Biotechnology, Middle East Technical University, 06800 Ankara, Turkey

F. A. Kaya · D. Uçkan
Pedi-Stem Center for Stem Cell Research and Development, Hacettepe University, 06100 Ankara, Turkey

B. B. Kuşkonmaz · D. Uçkan
Divison of Hematology, Department of Pediatrics, Hacettepe University, 06100 Ankara, Turkey

F. Severcan (✉)
Department of Biological Sciences, Middle East Technical University, 06800 Ankara, Turkey
e-mail: feride@metu.edu.tr

Introduction

A stem cell is a special kind of cell that has a unique capacity to renew itself and to give rise to specialized cell types (Pittenger et al. 1999). Mesenchymal stem cells (MSCs) are present in a variety of tissues, and they have the potential to differentiate into specific lineages that are mainly chondrocytes, osteoblasts, adipocytes,

fibroblasts, marrow stroma, and other tissues of mesenchymal origin. These cells are isolated according to their plastic adherence capability, and they can be differentiated in vitro into adipocytes, osteocytes, and chondrocytes (Baxter et al. 2004). MSCs have gained significant importance in regenerative medicine for the last decade, because of the ease of their isolation, differentiation potential, immunosuppressive properties, and availability for autologous and allogenic transplantation (Pittenger et al. 1999; Aggarwal and Pittenger 2005).

MSCs in specific organ systems are required for the maintenance and repair of the tissues throughout adult life. This function of stem cells is regulated by molecular signaling to ensure proper cellular, tissue, and organ homeostasis, but how this coordination changes with aging is mostly unknown (Drummond-Barbosa 2008). The reciprocal interactions between stem cell aging on tissue homeostasis and aged cellular microenvironment on stem cells will be critical to the success of any therapeutic application of stem cells in the emerging field of regenerative medicine (Rando 2006; Drummond-Barbosa 2008).

The process of MSC aging is important because of their role in tissue regeneration and repair. In order to achieve favorable clinical outcome with cellular therapy, the impact of age on MSCs has to be understood clearly (Wilson et al. 2010). Existing studies have focused on the effect of aging on the differentiation ability or on the number of colony-forming unit fibroblast (CFU-F) to study the proliferation capacity of MSCs. Some, but not all studies showed that aging reduces osteogenesis, chondrogenesis, and adipogenesis (Zheng et al. 2007; Tokalov et al. 2007). In these studies, decrease in the number of MSCs in the bone marrows of rodents, monkeys, and humans were reported. Furthermore, the studies in the literature showed that MSCs of older donors revealed decreased proliferation potential and increased senescence when compared with the cells of younger donors (Baxter et al. 2004; Mareschi et al. 2006). It was suggested that aging is associated with a decrease in the number and function of stem cells (Baxter et al. 2004; Mareschi et al. 2006). However, causal relationship is largely unknown. Despite available information, little is known about how and why MSCs age in vivo. The effects of donor age in regenerative medicine and in vivo use for wound healing have not been investigated in detail, so far. It is proposed that donor age may have a significant impact on the efficacy of stem cell treatments. Stem cells can be differentiated into many different types of cells. Determination of the molecular differences in stem cells depending on the donor age may contribute to better selection of donors in regenerative medicine, development of in vitro conditions for stem cell-based clinical applications. Thus, understanding of the cellular, biochemical, and molecular interactions between MSCs and their microenvironment and other stem cells will contribute to development of better in vitro modeling strategies for stem cell studies.

Fourier transform infrared (FTIR) spectroscopy is a non-disturbing, non-invasive technique which provides quantitative and structural information about biological samples (Cakmak et al. 2011). It gives valuable information about the biological samples by detecting changes in the functional groups belonging to the tissue or cell components such as lipids, proteins, carbohydrates, and nucleic acids, simultaneously (Kneipp et al. 2000; Cakmak et al. 2011). The shifts in the band frequencies, changes in the bandwidth, and band area/intensity values provide valuable information that is correlated with the alterations in the structure and composition of macromolecules (Naumann 2001). FTIR spectroscopy has become a valuable tool for diagnosis in medicine (Leskovjan et al. 2010; Severcan et al. 2010). This technique is used to determine the effect of radioprotectant in irradiated tissues (Cakmak et al. 2011), taxonomical studies in microbiology (Dogan et al. 2007), plant studies (Gorgulu et al. 2007), discrimination of drug-resistant and drug-sensitive cancer cells (Gaigneaux et al. 2006), and examination of apoptosis (Di Giambattista et al. 2011), and it is also recently used in determination of differentiation of stem cells (Ishii et al. 2007) and characterization of substrates related with stem cell growth and labeling (Krafft et al. 2007; Aksoy et al. 2012). Attenuated total reflection (ATR) mode of FTIR spectroscopy is a powerful tool to study biomedical samples. In this technique, sample preparation procedure is reduced, because the samples can directly be placed on an ATR crystal before spectral measurements have been performed (Kazarian and Chan 2006).

FTIR microspectroscopy (FTIRM) can be defined as a combination of an infrared spectroscopy with a microscope. It provides spatially resolved information on unstained thin tissue samples or cell monolayers by allowing the generation of IR images with high image contrast (Cakmak et al. 2012). Unlike staining techniques, IR microcopy with its label-free, non-invasive, and non-destructive properties generates information

about relative concentrations and structure of macromolecules by considering alterations in the infrared spectra and the specific heterogeneties (Bechtel et al. 2009; Cakmak et al. 2011). In this context, FTIR imaging contains a multiplicity of contrast yielding mechanisms that are derived from variations in the chemical composition, without the addition of extrinsic markers or stains. IR microspectroscopy of biological systems is a developing area to investigate cells in different stages such as their growth cycles (Matthaus et al. 2006), cancerous states (Dukor 2002), and contaminated states with pathogens (Erukhimovitch et al. 2005).

The use of MSCs in the field of hematology holds promise, since these cells provide supportive environment for cells of the hematopoietic system. The current study was designed to investigate age-related differences in MSCs that may be useful in donor selection in allogenic stem cell transplantation as well as in other stem cell therapies. In this context, the present study was intended to identify new molecular marker(s) reflecting the effects of aging on BM-MSCs that were obtained from different aged healthy bone marrow donors. For this purpose, ATR-FTIR spectroscopy and FTIR microspectroscopy were used together to evaluate the results by standard statistic and chemometric methods. The spectral results of each sampling group were discriminated by cluster analysis according to their variations. This analysis not only offers the opportunity to differentiate between sampling groups but also tests the interpoint distances between all samples.

Results

In the present study, molecular level differences or similarities between healthy BM-MSCs from different age groups were investigated initially by ATR-FTIR spectroscopy followed by FTIR microspectroscopy and hierarchical cluster analysis. The spectral results of each group were statistically compared with the remaining four groups in order to reveal the differences between them.

BM-MSCs were characterized by their adherence to plastic surface of culture flask, their fibroblast-like morphology under inverted light microscope, and according to their phenotypic and differentiation characteristics in accordance with International Society for Cellular Therapy (ISCT) criteria (Dominici et al. 2006). As can be seen from Fig. 1, BM-MSCs from all groups showed similar morphology; they were positive for CD105,

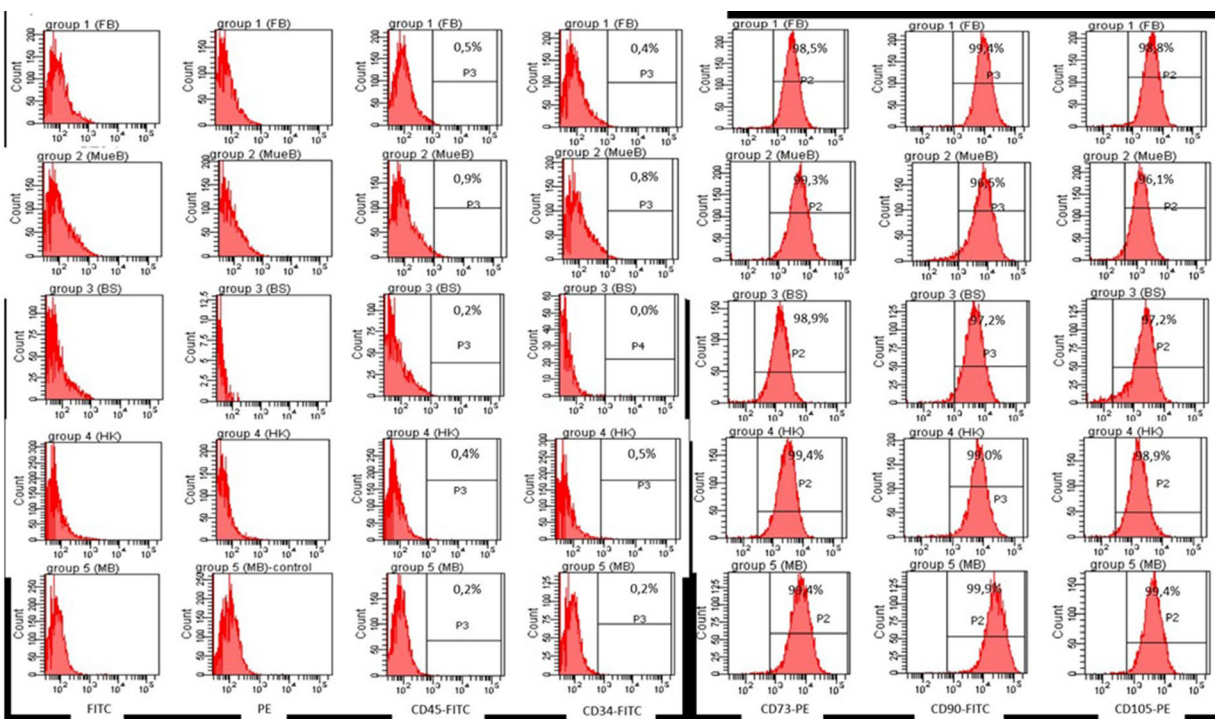

Fig. 1 The results of surface antigen profiles of healthy BM-MSCs belonging to five different age groups

CD73, and CD90 antigens in ≥95 % while they lacked expression of hematopoietic markers including CD45 and CD34. According to definitions of ISCT, BM-MSCs must have capacity to differentiate into at least osteoblasts and adipocytes by standard differentiation-inducing media (Dominici et al. 2006). Adipogenic and osteogenic differentiation was assessed by using Oil Red O and Alizarin Red staining, respectively. As can be seen in Fig. 2a, b, there were decreases in the adipogenic and osteogenic differentiation potentials in early and mid adults (ages >20–50 years) when compared with the younger donors (range of ages 0–19 years) visually.

Figure 3 shows the phosphate-buffered saline (PBS) buffer-subtracted general representative FTIR spectra of healthy human BM-MSCs from different age donors in the 3,800–800 cm^{-1} spectral region. The spectrum contains several bands representing many different functional groups of lipids, proteins, carbohydrates, and nucleic acids. The positions of these bands are assigned in Table 1. The spectra of BM-MSCs from different age groups were analyzed in two major regions as 3,000–2,800 and 1,800–800 cm^{-1}. The baseline-corrected average spectra were used to perform accurate measurements of the spectral parameters like band frequencies and band areas. All spectra presented in the figures were normalized with respect to the amide A band centered at around 3,330 cm^{-1} for illustrative purposes. Numerical variation of band area values are listed in Table 1.

Figure 4 represents FTIR spectra of BM-MSCs from five different age groups in the 3,000–2,800 cm^{-1} region that was used to determine the level of saturation in the lipid acyl chains by examining the changes in the CH_3, CH_2 antisymmetric, and CH_2 symmetric stretching bands (Severcan et al. 2005; Leskovjan et al. 2010). The variations in the area under the spectral bands give information about concentration of the functional groups belonging to the relevant molecule; for example,

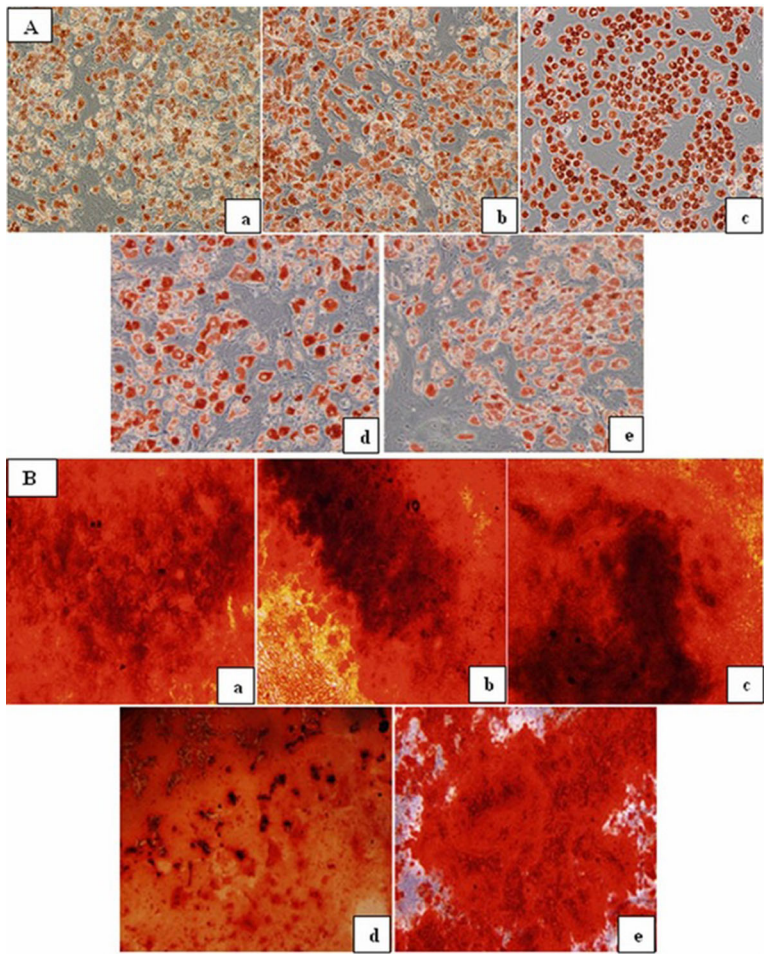

Fig. 2 **a** Oil Red O staining of healthy P3 BM-MSCs at the end of 21 days—infant MSCs (*a*), children MSCs (*b*), adolescent MSCs (*c*), early adult MSCs (*d*), and mid adult MSCs (*e*) (magnification=×20). **b** Alizarin Red staining of healthy P3 BM-MSCs at the end of 21 days—infant MSCs (*a*), children MSCs (*b*), adolescent MSCs (*c*), early adult MSCs (*d*), mid adult MSCs (*e*) (magnification=×20)

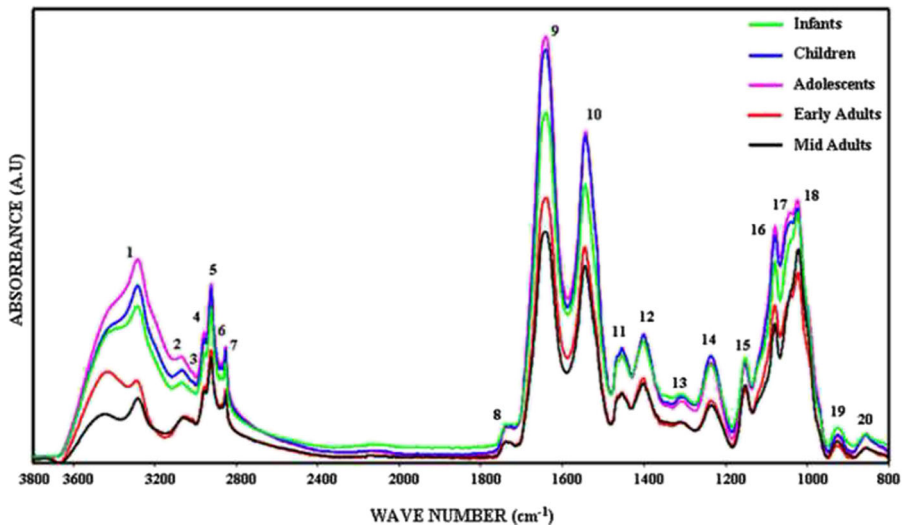

Fig. 3 The representative infrared spectra of healthy BM-MSCs from different age donors. *Green line* represents infant BM-MSCs; *blue line* represents children BM-MSCs; *pink line* represents adolescent BM-MSCs; *red line* represents early adult BM-MSCs; and *black line* represents mid adult BM-MSCs in the 3,800–800 cm^{-1} region (the spectra were normalized with respect to the amide A band) (color figure online)

the increase in the band area values represent an increase in the concentration of assigned molecule (Cakmak et al. 2006, 2011; Severcan et al. 2005). The band area values of the CH_3 antisymmetric stretching band at 2,957 cm^{-1} was significantly higher in the children ($p<0.01$) and adolescent ($p<0.001$) groups with respect to the infant group. The area of this band decreased significantly in early adult ($p<0.01$) and mid adult BM-MSCs ($p<0.01$) in comparison to the area of children group BM-MSCs. Additionally, a significant decrease was also present in early adults ($p<0.001$) and mid adults ($p<0.001$) when compared with the area of adolescent BM-MSCs (Table 1). The area of CH_2 antisymmetric stretching band of BM-MSCs increased significantly in the children ($p<0.001$) and the adolescent groups ($p<0.001$) with respect to the infants. Meanwhile, the area of the band was significantly lower in early adults ($p<0.001$) and mid adults ($p<0.001$) when compared with the area of children and adolescent BM-MSCs (Table 1). The CH_2 symmetric stretching band area was higher in adolescent group BM-MSCs ($p<0.01$) with respect to infants. The band area degrees were lower in early adult ($p<0.01$) and mid adult BM-MSCs ($p<0.05$) with respect to the children group. The band area value of BM-MSCs from mid adults decreased significantly ($p<0.05$) when compared with the area value of adolescent group (Table 1). The increase in saturated lipid concentration in the infant, children, and adolescent groups was further supported by the increase in the area of CH_2 bending vibrations of lipids, at 1,453 cm^{-1} (Di Giambattista et al. 2011), and COO^- symmetric stretching vibrations of fatty acid side chains, at around 1,400 cm^{-1} (Table 1) (Peuchant et al. 2008; Cakmak et al. 2006). Such an increase in the saturated lipid contents may indicate an increase in lipid synthesis in younger cells as a result of increased cellular proliferation.

Figure 5 represents the 1,800–800 cm^{-1} spectral region containing vibrational modes of several distinct functional groups belonging to lipids, proteins, carbohydrates, and nucleic acids. The bands located at 1,639 and 1,545 cm^{-1} are assigned to C=O stretching and N–H bending (amide I) and N–H bending and C–N stretching (amide II) vibrational modes of structural proteins, respectively. Changes in the band areas of amide I and amide II reflect an alteration in the protein concentrations in cells (Manoharan et al. 1993; Haris and Severcan 1999). As can be seen in Fig. 5 and Table 1, amide I and amide II band area values of BM-MSCs were significantly higher ($p<0.001$) in children and adolescents ($p<0.001$) than infant, early adult, and mid adult groups. However, significant decreases were observed in the amide I band area of early adult BM-MSCs ($p<0.001$) and mid adult BM-MSCs ($p<0.001$) with respect to the area of children group. The amide I band area of BM-MSCs also decreased significantly in mid adults ($p<0.001$) according to the adolescents. Amide II band area value of BM-MSCs of adolescents was significantly higher ($p<0.001$)

Table 1 The band area values of healthy BM-MSCs from five different age groups

Band area values[a]							
Band numbers	Wave numbers (cm^{-1})	Assignments of the bands	Infants (n=5)	Children (n=5)	Adolescents (n=5)	Early adults (n=5)	Mid adults (n=5)
3	3,015	Olefinic =CH stretching	0.046±0.01	0.046±0.002	0.066±0.01 ↑	0.04±0.004	0.04±0.004
4	2,954	CH_3 antisymmetric stretching	0.85±0.022	1.08±0.047** ↑	1.18±0.059*** ↑	0.89±0.042††,### ↓	0.84±0.015††,### ↓
5	2,924	CH_2 antisymmetric stretching	2.09±0.064	2.57±0.048*** ↑	2.82±0.029*** ↑	1.99±0.119†††,### ↓	1.93±0.026†††,### ↓
6	2,873	CH_3 symmetric stretching	0.26±0.011	0.33±0.016* ↑	0.35±0.023** ↑	0.25±0.009†,## ↓	0.25±0.012†,### ↓
7	2,852	CH_2 symmetric stretching	0.61±0.013	0.68±0.021	0.71±0.02** ↑	0.61±0.022†† ↓	0.60±0.009†,### ↓
8	1,740	C=O stretching	0.35±0.019	0.38±0.014	0.39±0.008	0.34±0.017	0.34±0.01
9	1,639	Amide I	12.92±0.408	16.13±0.249*** ↑	17.87±0.646***,† ↑	12.01±0.285††† ↓	11.41±0.193†††,### ↓
10	1,545	Amide II	10.60±0.945	12.52±0.163	13.44±0.552** ↑	9.02±0.181†††,### ↓	8.49±0.228†††,### ↓
11	1,453	CH_2 bending vibration	2.77±0.184	3.02±0.271	3.15±0.11	2.17±0.063†,## ↓	2.13±0.113††,### ↓
12	1,402	COO^- symmetric stretching	3.77±0.308	4.38±0.135	4.41±0.143	3.61±0.221	3.50±0.161†,# ↓
13	1,310	Peptide side chain vibrations	2.42±0.19	2.70±0.178	2.73±0.109	2.27±0.05	2.20±0.059†,# ↓
14	1,234	PO_2^- antisymmetric stretching	3.89±0.23	4.84±0.117** ↑	4.87±0.101** ↑	3.54±0.33†††,### ↓	3.44±0.182†††,### ↓
15	1,152	CO–O–C antisymmetric stretching	2.63±0.119	2.69±0.112	2.75±0.087† ↑	2.17±0.101*,††,## ↓	2.12±0.084*,††,## ↓
16	1,080	PO_2^- symmetric stretching	3.12±0.054	3.76±0.146	3.85±0.171	3.07±0.242# ↓	2.90±0.194†,# ↓
17	1,045	CO stretching vibrations	3.72±0.096	4.50±0.139** ↑	4.74±0.149*** ↑	2.94±0.111**,†††,### ↓	3.09±0.075*,†††,### ↓
18	1,025	Mainly from glycogen	3.62±0.32	4.74±0.292** ↑	5.52±0.119*** ↑	3.47±0.227††,### ↓	4.14±0.151## ↓
19	925	DNA-Z form	0.20±0.009	0.24±0.014	0.29±0.01** ↑	0.23±0.011# ↓	0.22±0.02## ↓
20	855	Nucleic acid-related vibrations	0.10±0.009	0.15±0.021	0.20±0.033*↑	0.15±0.012	0.10±0.022# ↓

[a] The band area values were shown as "mean±standard error" for each group. The degree of significance was denoted as follows: *p<0.05, **p<0.01, ***p<0.001 with respect to the infants; †p<0.05, ††p<0.01, †††p<0.001 with respect to the children; #p<0.05, ##p<0.01, ###p<0.001 with respect to the adolescents

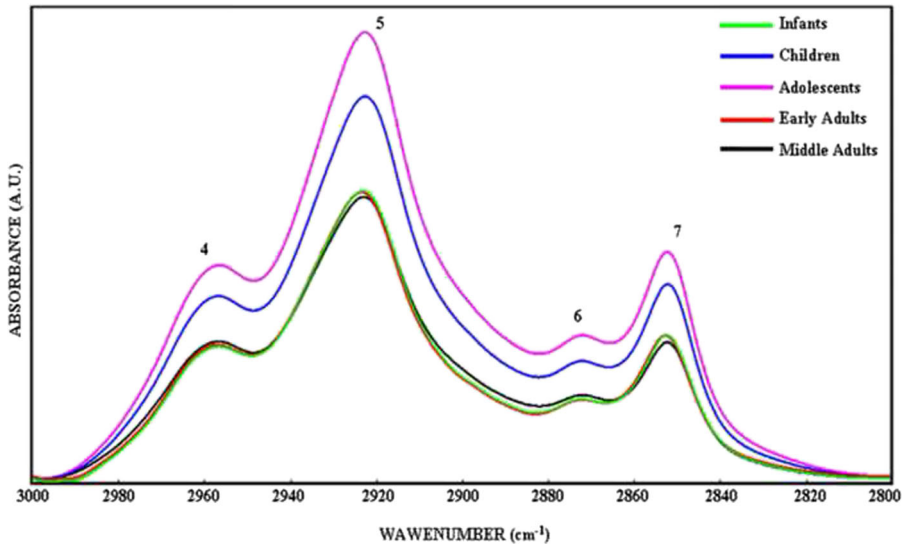

Fig. 4 The representative infrared spectra of healthy BM-MSCs from five different age groups in the 3,000–2,800 cm^{-1} region. *Green line* represents infant BM-MSCs; *blue line* represents children BM-MSCs; *pink line* represents adolescent BM-MSCs; *red line* represents early adult BM-MSCs; and *black line* represents mid adult BM-MSCs (the deconvolved spectra were normalized with respect to the amide A band) (color figure online)

than the value of infants. The area of amide II band was significantly lower in early adults ($p<0.001$) and mid adults ($p<0.001$) according to the children and adolescent BM-MSCs.

The strong bands at 1,234 and 1,080 cm^{-1} arise from antisymmetric and symmetric stretching vibrations of phosphodiester groups that are present in the phosphate moieties (PO_2^-) of nucleic acid backbone structures and phospholipids (Rigas et al. 1990). Children and adolescent BM-MSCs showed significantly ($p<0.01$) higher PO_2^- antisymmetric stretching band area values with respect to the infant BM-MSCs. The band area values for PO_2^- antisymmetric stretching band in early and mid adult BM-MSCs were significantly lower ($p<0.001$) when compared to the children and adolescent values. Similar band area alterations were observed in the PO_2^- symmetric stretching band at around 1,080 cm^{-1}. The area of this band decreased in early

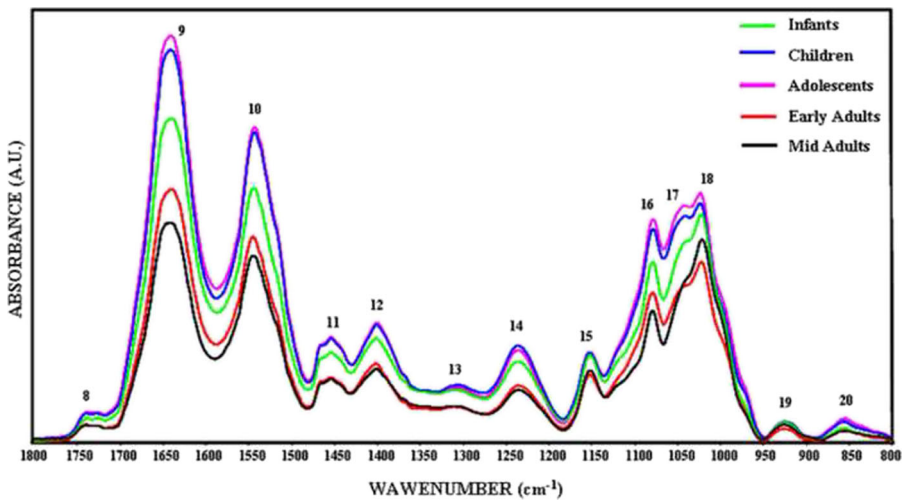

Fig. 5 The representative infrared spectra of healthy BM-MSCs from five different age groups in the 1,800–800 cm^{-1} region. *Green line* represents infant BM-MSCs; *blue line* represents children BM-MSCs; *pink line* represents adolescent BM-MSCs; *red line* represents early adult BM-MSCs; and *black line* represents mid adult BM-MSCs (the spectra were normalized with respect to the amide A band) (color figure online)

adults and mid adult BM-MSCs ($p<0.05$) with respect to the children and adolescent values.

The area of the band at 1,152 cm^{-1}, which is due to stretching mode of the C–O–O–C groups existing in glycogen and nucleic acids (Rigas et al. 1990), was higher in children and adolescent BM-MSCs. The band areas of early adult ($p<0.01$) and mid adult ($p<0.01$) BM-MSCs tended to decrease significantly when compared with the band area values of infant, children, and adolescent BM-MSCs. The other two bands located at about 1,025 and 1,045 cm^{-1} are attributed from the vibrational frequency of $–CH_2OH$ groups and the C–O stretching frequencies coupled with C–O bending frequencies of the C–OH groups of carbohydrates (including glucose, fructose, glycogen, etc.) (Parker 1971). As can be seen in Table 1, while increase in the area values of 1,045 cm^{-1} band of children ($p<0.01$) and adolescents ($p<0.001$) were significant with respect to infant BM-MSCs, the values of early adult ($p<0.01$) and mid adult ($p<0.05$) BM-MSCs were significantly lower than those from infants. Significant decreases in the area of this band in early adult ($p<0.001$) and mid adult ($p<0.001$) BM-MSCs were observed when they were compared to the band area values of children and adolescent BM-MSCs. Children ($p<0.05$) and adolescent ($p<0.001$) BM-MSCs had also significantly higher band area values for 1,025 cm^{-1} band than infants. On the contrary, early adult ($p<0.01$ and $p<0.001$) and mid adult ($p<0.01$) BM-MSCs had lower band areas than children and adolescent BM-MSCs, respectively.

The two bands at about 925 and 855 cm^{-1} are assigned to sugar vibrations in left-handed Z-type DNA (Dovbeshko et al. 2000) whose area increased in adolescent BM-MSCs significantly ($p<0.05$ and $p<0.01$, respectively) according to the infant values. However, in early adult ($p<0.05$) and mid adult BM-MSCs ($p<0.05$), band area values decreased significantly with respect to the adolescent BM-MSCs.

Thiazolyl blue tetrazolium bromide (MTT) proliferation assay was used to support ATR-FTIR spectroscopy results which reflects global alterations in the concentrations of different macromolecules of passage 3 BM-MSCs. MTT proliferation assay is based on the cleavage of the yellow MTT (3-(4.5-dimethylthiazol-2-yl)-2.5-diphenyltetrazolium bromide, a tetrazole) salt to purple formazan crystals in the mitochondria of metabolically active and highly proliferative viable cells (Van de Loosdrecht et al. 1994). In the present study, BM-MSCs of five different sample groups were compared in terms of their cellular activity by MTT assay for 11 days. Metabolic and cell proliferation activities of BM-MSCs were measured at days 1, 3, 5, 7, 9, and 11 by measuring the purple solution of formazan crystals in sodium dodecyl sulfate (SDS) by spectrophotometry at 620-nm wavelength. Statistical analysis results of MTT proliferation assay are shown in Table 2; at day 3, the metabolic and cellular activity of mid adult group decreased significantly with respect to the children and adolescent groups. At day 5, the metabolic and cellular activity of adolescent group showed significant increase with respect to the infant group, while the metabolic and cellular activity of early adult group decreased significantly with respect to the adolescent group; also, metabolic and cellular activity of the mid adult group showed significant decrease with respect to the children and adolescent groups. At day 7, the metabolic and cellular activity of

Table 2 MTT proliferation assay results of healthy BM-MSCs obtained from five different age groups

Absorbance[a]					
Days	Infants	Children	Adolescents	Early adults	Mid adults
1	0.148±0.002	0.157±0.014	0.167±0.002	0.141±0.011	0.132±0.005
3	0.165±0.004	0.171±0.005	0.179±0.002	0.156±0.007	0.150±0.002†,### ↓
5	0.173±0.005	0.177±0.002	0.188±0.001* ↑	0.163±0.006## ↓	0.158±0.004††,### ↓
7	0.179±0.032	0.183±0.006	0.195±0.003	0.169±0.001### ↓	0.165±0.003
9	0.185±0.003	0.191±0.003	0.21±0.003**,†† ↑	0.176±0.003***,†,## ↓	0.170±0.003*,†††,### ↓
11	0.180±0.006	0.196±0.015	0.214±0.004* ↑	0.179±0.008# ↓	0.173±0.003# ↓

[a] The values were shown as "mean±standard error" for each group. Each group were compared to one another for each day separetely. The significancies were only obtained with respect to the infant, children, and adolescent groups. The degree of significance was denoted for each day as follows: *$p<0.05$, **$p<0.01$, ***$p<0.01$ with respect to infants; †$p<0.05$, ††$p<0.01$, †††$p<0.01$ with respect to children; #$p<0.05$, ##$p<0.01$, ###$p<0.01$ with respect to adolescents

early adult group decreased significantly with respect to the children group. At day 9, adolescent group showed significant increase with respect to the infant and children groups, while early adults and mid adults showed significant decrease with respect to the infant, children, and adolescent groups. At day 11, adolescent group showed significant increase with respect to the infant while early adults and mid adults showed significant decrease with respect to the adolescent.

The specific integrated spectral regions for the infrared bands were used to determine distribution of functional groups in the FTIR spectral images. The average chemical maps were colored according to the peak integrated areas of CH_2 antisymmetric stretching, amide I, and PO_2^- antisymmetric stretching bands in order to observe distribution of lipids, proteins, and nucleic acids in BM-MSCs, respectively. Red color corresponds to the highest ratio, and blue color corresponds to the lowest ratio in the color bars that were stated in the chemical maps. As can be seen from the Fig. 6a–c, the concentrations of saturated lipids, proteins, and nucleic acids were higher in the children and adolescent groups when compared with the infants and early and mid adults supporting the ATR-FTIR spectroscopy empirical results.

FTIR imaging was used as a supportive method for ATR-FTIR spectral results which provides visual representation of the variations in the molecular content and concentration. The differences in the distribution of concentration of lipids, proteins, and nucleic acids in MSCs of five different age groups were demonstrated representatively. The intensity/area changes of the CH_2 antisymmetric stretching band gives an information about saturated lipid concentration in the system (Severcan et al. 2003, Cakmak et al. 2006). We constituted the chemical maps of saturated lipids by using the peak integrating maps of the CH_2 antisymmetric stretching band. In order to observe the changes in concentrations of proteins, we constituted the chemical map by using the area distribution of bands which arises mainly from the C=O stretching and N–H bending vibration of the amide I band (Manoharan et al. 1993, Haris and Severcan 1999). In addition to these bands, the integrated band area distribution of PO_2^-

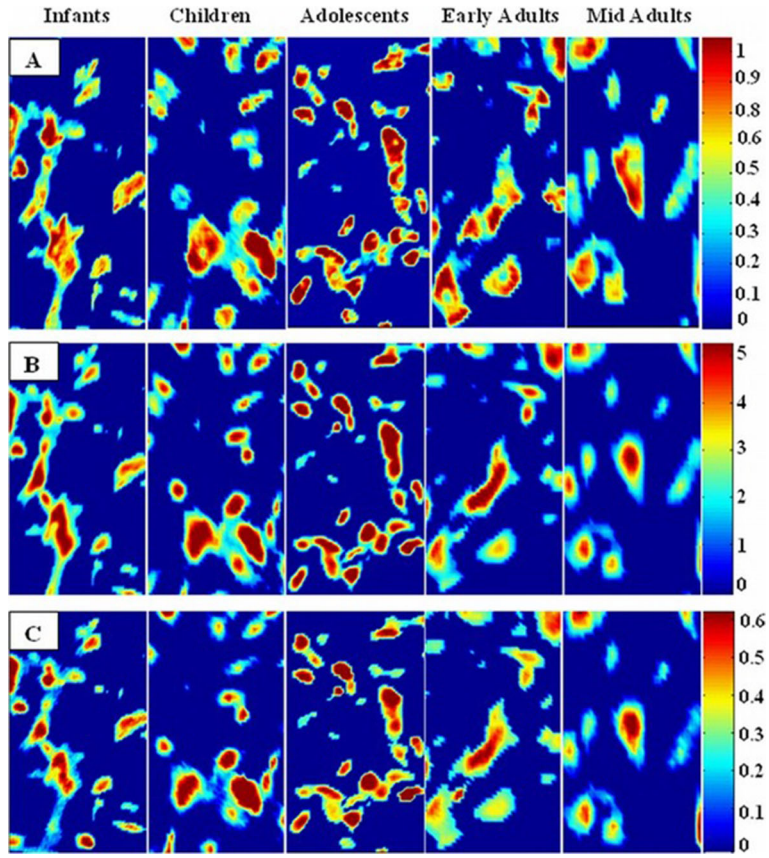

Fig. 6 Spectral image maps that reflect distribution of lipids, proteins, and nucleic acids in the BM-MSCs from five different age groups. These maps were derived respectively by taking the peak integrated areas of **a** CH_2 antisymmetric stretching bands of lipids, **b** amide I band of proteins, and **c** PO_2^- antisymmetric stretching bands of nucleic acids

antisymmetric stretching of nucleic acids was used to make a chemical map of nucleic acid changes in the cells (Rigas et al. 1990). The concentrations of saturated lipids, proteins, and nucleic acids of BM-MSCs in children and adolescent groups were higher when compared with the infants, early adults, and mid adults (Fig. 4a–c). The average chemical maps were colored according to the intensity/area values of mentioned bands where red color corresponds to the highest ratio and blue color corresponds to the lowest ratio as shown on the color bar in the figures. As it was understood from the color changes in these chemical maps, concentrational changes can be ordered from higher to lower values as adolescents, children, infants, ealy adults, and mid adults.

Finally, hierarchical cluster analysis was performed to compare BM-MSCs of infants, children, adolescents, early adults, and mid adults based on their spectral differences in ATR-FTIR. The analysis was applied to vector-normalized 29 independent spectra of five sampling groups in two different regions, namely, 3,000–800 and 1,800–800 cm^{-1}. As depicted in Fig. 7a, five different clusters were produced with a high accuracy of success for infants (4/6), for children (6/6), for adolescents (6/6), for early adults (6/6), and for mid adults (5/5), respectively, for 3,000–800 cm^{-1} spectral region. The heterogeneity value was 1.4 and two samples from infant group that were marked with asterisk (*) mixed into the children group. Additionally, as can be seen in Fig. 7b, different clusters were produced with a high accuracy of success for infants (6/6), for children (5/6), for adolescents (6/6), for early adults (6/6), and for mid adults (5/5), respectively, for 1,800–800 cm^{-1} spectral region with the heterogeneity value 3. Only one sample from the children group that was marked with number sign (#) mixed into the infant group. As can be seen from the dendrograms, all samples were successfully differentiated into the five different clusters.

Discussion

There has been limited information about how donor age affects the fate of stem cells and whether the changes caused by aging alter the stem cell niche (Campisi and Sedivy 2009). It is hypothesized that impaired tissue homeostasis and regeneration capacity may arise from alterations in the number and/or function of stem cells (Rando 2006). In this context, the question arises whether age-related changes are due to the intrinsic aging of stem cells or due to the aged stem cell microenvironment (niche) (Wagner et al. 2008). There is a need for investigation of age-related alterations in stem cells and their external environment in order to standardize quality products and cellular therapies. The effects of the number of passages and population doublings on cell aging and senescence-associated molecular changes are not clearly defined, particularly when their influence on cellular therapies are considered. These findings make it inevitable to define a reliable and easy method to track cellular aging of MSCs (Wagner et al. 2010). Studies in

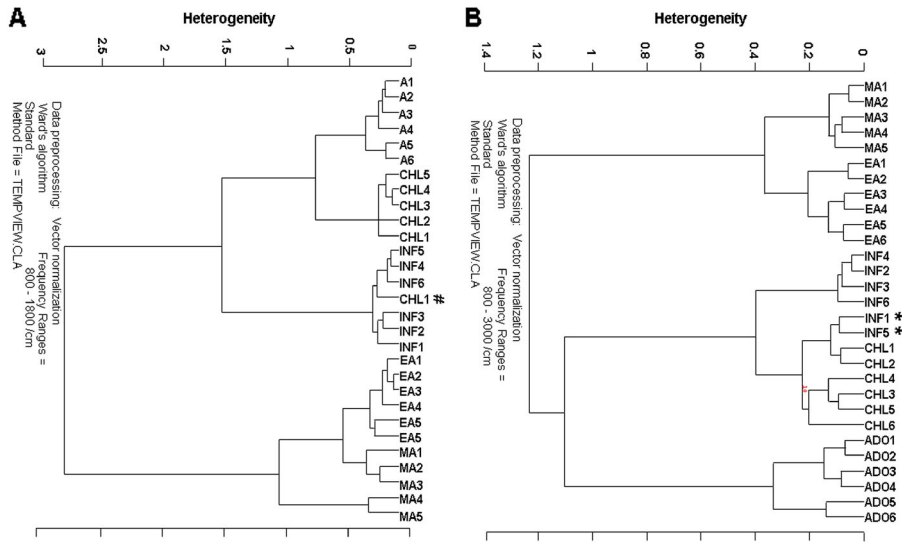

Fig. 7 Hierarchical cluster analysis performed on the vector-normalized spectra of BM-MSCs of infants, children, adolescents, early adults, and mid adults and resulting from Ward's algorithm. The study was conducted in the **a** 1,800–800 and **b** 3,000–800 cm^{-1} spectral regions

the literature have reflected that cellular senescence does not significantly affect the viability, morphology, function, proliferation, and differentiation capacity of cells, while it causes decline in cellular metabolism (Wagner et al. 2008, 2010). Until now, senescence-associated β-galactosidase (SA-β-gal) has been used to determine senescence. Although SA-β-gal is overexpressed and accumulates specifically in senescent cells, it is not considered as a specific marker of senescence. The enlarged and apoptotic cells in higher passages also become SA-β-gal-positive, suggesting that β-galactosidase activity is associated with mainly replicative senescence in vitro (Wagner et al. 2010). Therefore, at present, a specific molecular marker to indicate the degree of cellular aging in MSCs is lacking. In this context, the present study suggested that infrared spectroscopy as a novel and non-destructive research method with its real-time chemical monitoring and high-quality data collection properties can be used to identify molecular marker(s) reflecting the stem cell aging.

In the present study, bone marrow samples from adult and aged donors who are older than 50 years old were not available. In the current hematopoetic stem cell transplantation (HSCT) practice in adult and aged donors, the use of granulocyte colony stimulating factor (GCSF)-mobilized peripheral blood stem cells (PBSC) is the preferred stem cell source due to the ease of collection and the lack of the need for general anesthesia. Therefore, bone marrow harvest is rarely used in aged adults, and the samples above 50-year-old donors were not used in this study for comparison. On the other hand, bone marrow harvest from sibling donors of pediatric age still remains as a common practice in family transplants. Therefore, bone marrow from healthy donors is practically available in pediatric practice of HSCT, where most donors are of young age as opposed to adult HSCT where stem cell source is GCSF-mobilized peripheral blood rather than bone marrow. For this reason, all healthy donors greater than 50 years old found in the cell collection of our stem cell center had received GCSF for mobilization of peripheral blood stem cells; therefore, advanced age subjects were not included in the study.

In our study, passage 3 BM-MSCs obtained from different aged donors showed similar morphology in terms of their surface antigen characteristics. These results were in accordance with the study of Mareschi et al. (2006) where BM-MSCs of early adult donors (range of age 20–50) and pediatric donors (range of age 6–11) were compared until passage 10. The study by Huang et al. (2005) demonstrated that BM-MSCs of fetuses, 0–20-, 20–40-, and >40-year-old donors, had similar morphology and antigenic phenotype. In the present study, adipogenic and osteogenic differentiation capacity of BM-MSCs was lower in adults (>20–50 years) when compared with the younger donors (ages 0–20). Kretlow et al. (2008) showed that chondrogenic, osteogenic, and adipogenic differentiation potentials of cells were decreased by aging.

The impairment of stem cell-based therapies can be caused by two factors as stem cell age and donor health. Aging is characterized by decline in the regenerative capacity and the function of stem cells resulting in less effective tissue homeostasis and repair (Raggi and Berardi 2012). Therefore, an understanding of MSC aging process is important for selecting most accurate donor to be able to increase the success of cellular therapies. The age-associated molecular changes in the cells include alterations in the proliferation rate, differentiation capability, genome stability, and expression profiles which means MSC aging is a complex, finely organized process at genomic, transcriptomic, epigenetic, and proteomic levels (Raggi and Berardi 2012; Harris 2012). The present ATR-FTIR and FTIR imaging studies showed that the changes in the concentration of essential molecules in BM-MSCs were interpreted as alterations in the proliferation capacity of the cells caused by donor aging. According to the results of ATR-FTIR study, the concentration of proteins, saturated lipids, carbohydrates, and nucleic acids decreased in the early and mid adults that were associated with the decline in the cell proliferation rate and bone marrow activity which were also supported by MTT proliferation assay results. Especially in early, mid, and older adults, stem cells reduced or ceased their growth and regeneration capacities to maintain tissue homeostasis or to reduce cancer development risk in aging tissues (Signer and Morrison 2013). Additionally, the current findings in the literature suggest that such biochemical changes in the stem cell niches are responsible for regenerative declines in older mammalians (Conboy and Rando 2012). The MTT assay results of the present study showed that metabolic and cellular activity of the early and mid adult BM-MSCs decreased, such a decrease in the mitochondrial activity, growth, and metabolic rates of the cells of mammalian tissues can influence the rates of the cellular aging at the later stages of the life (Dillin et al. 2002).

Human MSCs with their multilineage differentiation ability and self-renewal capacity have great potential as a source of cells for cellular therapies in regenerative medicine and for tissue engineering approaches (Baksh et al. 2004). BM-MSCs provide housing for HSCs and enhance their engraftment after HSC transplantation (Lazarus et al. 2005) which has been used for some years in the treatment of leukemia and other cancers (Tabbara et al. 2002). Therefore, the use of MSCs in stem cell therapies requires standardization and quality control of each step from isolation to transplantation (Wagner et al. 2010). The present study aimed to investigate the effect of healthy donor age on the quality of the BM-MSCs at molecular level by considering the available data in the literature about the negative impacts of the MSC donor age and the disease status of the donor in terms of their clinical utility and the success of the clinical outcomes (Harris 2012). The results of our ATR-FTIR and imaging study showed significant decreases in the proliferation capacity and the bone marrow activity of the early and mid adult BM-MSCs while the proliferation activity were higher in younger BM-MSCs obtained from infants, children, and adolescents. These spectral results were also supported by the successful discrimination of the different age groups via cluster analysis. The higher heterogeneity values were obtained by the cluster analysis which implied presence of important molecular alterations among BM-MSCs of different age groups. As can be seen in Fig. 7a, b, MSCs of early and mid adult groups were separated in the same branch of the dendrogram, while MSCs of infant, children, and adolescent groups which were separated in the other branch of the dendrogram together which reflected the differences between older and younger donor groups. According to the results of ATR-FTIR spectroscopy and FTIR imaging together with the results of cluster analysis, it is suggested that the MSCs obtained from older adult donors with lower proliferation rate and regenerative capacity may have disadvantages. On the other hand, the cells obtained from infants, children, and adolescents have significantly higher proliferative capacity, but there are ethical issues to be considered when using children donors. Generally, elder donor is selected if there are several donor candidates in a family for HSCT. However, in pediatric transplants, HLA-matched donor is usually the sibling of the child who is of young age but ethical limitations for use of children's materials restrict the use of young donors for transplant or for research. The study subjects in the present study were all family donors, and ethical approval was obtained to use a very small amount of the harvested material for MSC expansion. Here, the advantage of ex vivo expansion of MSCs may enable the use of those young donors with small volume of starting samples obtained from bone marrow harvest products. However, in order to obtain sufficient number of therapeutic cells from 1–3 ml of starting sample volumes, there is a need for improvement of MSC ex vivo expansion protocols. Our supportive cluster analysis results especially reflected that the infant, children, and adolescent groups were discriminated as in different clusters of the same branch of the dendrogram. For cellular therapy process, if there is choice chance when selecting the appropriate donor cells with very small starting volumes, infant and children groups may be preferred for each other by considering closeness of their clusters in the same branch (Fig. 7b). Similarly, if there is a choice option when selecting the appropriate donor, children and adolescent groups may be preferred for each other by considering closeness of their clusters in the same branch (Fig. 7a). It has been shown that increased donor age in human bone marrow can cause changes in the both MSC properties and also HSCs that are closely interacted with each other. The increased donor age in bone transplantation is a predictor of transplant-related mortality, consistent with the cell-autonomous HSC defects, maintenance, and stress responses of the HSCs (Tower 2012). The study of Jinui and colleagues (Harris 2012) showed that aging mice transplanted with MSCs from young donors had prolonged life span by 15 to 20 %. In contrast, MSCs isolated from the older donor animals failed to prolong life span at all, showing significantly less capability to differentiate into bone, fat, neural, and muscular cells as compared to MSCs from younger animals. The other study performed by Kollman and colleagues (2001) also reflected that age was the only donor trait significantly associated with overall and disease-free survival. The study of Kollman and colleagues (2001) showed that 5-year overall survival rates for recipients were higher in younger donors with respect to the older ones and the use of younger donors may lower the incidence of GVHD and improve survival after bone marrow transplantation.

All these results mean that stem cells collected from younger and healthier donors provide more successful therapeutics than the cells obtained from older donors. It seems that age-related changes in MSC properties should be taken into account whenever they are intended for application in cellular therapy or research.

Conclusion

In summary, the results of the study showed that donor age had significant influence on the concentrations of the essential molecules existing in the cells. The BM-MSCs from healthy donors in different ages had similar cellular morphology under inverted light microscope at passage 3. Also, their expression profiles for CD105, CD90, CD73, CD45, and CD34 surface antigens were the same. In addition to this, adipogenic and osteogenic differentiation potentials of early and mid adult BM-MSCs were found lower when compared to the younger infant, children, and adolescent group BM-MSCs with a visual evaluation under light microscopy. The spectral results reflected that there were significant increases in the concentration of saturated lipids, proteins, glycogen, and nucleic acids in children and adolescent group BM-MSCs when compared to the infants, early adults, and mid adults. The concentrations of mentioned molecules in early and mid adult BM-MSCs were significantly lower than the concentrations in the children and adolescent BM-MSCs. These increases in the concentrations of molecules might be due to an increase in the proliferation activity in younger BM-MSCs. FTIR microspectroscopy revealed the distribution of biomolecules in the cells as chemical maps whose results also are in agreement with the ATR-FTIR results. The cellular activity degree was determined through the MTT proliferation assay results, and this was used to support ATR-FTIR spectroscopy results. The MTT assay showed that BM-MSCs obtained from younger donors, such as infants, children, and adolescents, had higher cellular activity than the BM-MSCs obtained from early and mid adults. Based on the spectral differences, BM-MSCs of five different age groups were successfully discriminated from each other by applying the hierarchical cluster analysis to FTIR spectra. As a result of cluster analysis of two different spectral regions, the older and younger donor groups were separated in two different branches of the two dendrograms.

The current ATR-FTIR spectroscopy and imaging study together with hierarchical clustering can be used as a novel method to clarify the global alterations in structure and function of essential biomolecules in characterized BM-MSCs of different aged donors and to identify new molecular marker(s) in order to determine the effects of donor age on BM-MSCs.

Materials and methods

Sampling groups

Human bone marrow aspirates (3–5 ml) which were obtained from posterior iliac crest of healthy bone marrow transplantation donors were used as a source of BM-MSCs. Five different age groups classified as infants (0–3 years of age, $n=6$), children (ages >3–12, $n=6$), adolescents (ages >12–19, $n=6$), early adults (ages >19–35, $n=6$), and mid adults (ages >35–50, $n=5$) were analyzed. Marrow samples were obtained during the marrow harvest procedure after signing of informed consent that were prepared according to procedures approved by the ethics committee of the Bone Marrow Transplantation Unit, Hacettepe University Children's Hospital, Ankara, Turkey.

Isolation and cultivation of MSCs from human bone marrow samples

The isolation of BM-MSCs from different aged group healthy donors and their cultivation till passage 3 (P3) were performed according to the standard protocols (details reported in Aksoy et al. (2012)). These passage 3 BM-MSCs were used in all other detailed investigations that were performed in the scope of this study.

Flow cytometry

Flow cytometric analysis of P3 BM-MSCs were performed on a FACS Aria flow cytometer (Becton, Dickinson Biosciences, USA) to evaluate BM-MSCs in terms of expression of main MSC surface markers CD73 (BD Biosciences, USA), CD90 (BD Biosciences, USA), and CD105 (e-bioscience, USA) and lack of expression of HSC markers CD34 (BD Biosciences, USA) and CD45 (BD Biosciences, USA). All markers were conjugated with either fluorescent isothiocyanate (FITC) or phycoerythrin (PE). BM-MSCs were trypsinized and washed with PBS. To evaluate BM-MSC marker profile, 1×10^5 cells were suspended in 100-μl PBS-BSA-Na azide with 2 μl of each flow cytometry antibody in a separate tube for 30 min at dark. At the end of incubation time, cells were washed twice with PBS and finally diluted in 200-μl PBS-BSA-Na azide. The analysis of cells was performed according to 10.000 event count with the FACS Aria (Beckon Dickinson Biosciences, USA). The acquired data was

analyzed by using BD FACSDiva software v6.1.2 (Beckon Dickinson Biosciences, USA).

Adipogenic and osteogenic differentiation experiments

Passage 3 BM-MSCs from healthy donors were subjected to certain differentiation induction media to evaluate their stem cell potency by activating adipogenesis and osteogenesis.

Adipogenic differentiation

Confluent (90 %) cells from P3 of BM-MSC cultures in six-well plates were treated with 1 μM dexamethasone (Sigma, USA), 60 μM indomethacine (Sigma, USA), 500 μM IBMX (Sigma, USA), and 5 μg/ml insulin (Sigma, USA) in dulbecco's modified eagle's medium (DMEM-LG) (Biological Industries, Israil) with 10 % fetal bovine serum (FBS) (Gibco, USA). Medium was replaced every 3 days for a 3-week period, and adipogenesis was followed by microscopic investigation during 3-week period. Meanwhile, the cells in control wells were cultured for 3 weeks in DMEM-LG with 10 % FBS. At the end of differentiation period, cells were fixed with 10 % buffered formalin for 20 min at room temperature and stained with Oil Red O (Sigma, USA) for 10 min at room temperature to visualize adipogenic differentiation.

Osteogenic differentiation

Confluent (70–80 %) BM-MSCs from P3 in six-well plates were subjected to osteogenic medium composed of DMEM-LG (Biological Industries, Israil), 10 % FBS (Gibco, USA), 100 nM dexamethasone (Sigma, USA), 10 mM β-glycerophosphate (Sigma, USA), and 0.2 mM ascorbic acid (Sigma, USA). The induction medium of wells was replenished every 3 days, and also, osteogenesis was followed by microscopic investigation during 3-week period. Meanwhile, the cells in control wells were cultured for 21 days in low glucose DMEM with 10 % FBS. In order to visualize calcium deposits, cultures were stained with Alizarin Red solution (pH 4.2) after being fixed in 10 % formalin for 10–20 min at room temperature.

MTT proliferation assay

Passage 2 BM-MSCs of five different age group were seeded in a 96-well plate at a density of 1×10^4 cells/well in 200-μl complete medium, and the MTT assay was applied (Van de Loosdrecht et al. 1994). Cultured cells were expanded in 5 % CO_2 incubator at 37 °°C. One set of wells with MTT and culture medium without cells were used as a blank control. Twenty-microliter MTT (5 mg/ml in PBS) (Thiazolyl Blue Tetrazolium Bromide, Sigma-Aldrich, USA) solution was added to each well at days 1, 3, 5, 7, 9, and 11 of culturing. After addition of MTT, 96-well plate was covered with thin foil and incubated for 4 h at 37 °C in 5 % CO_2 incubator. Formazan crystals were observed as dark crystals at the bottom of plate under the inverted light microscope. At the end of the incubation period, 100 μl SDS (Sigma-Aldrich, USA) was added to each well and incubated at room temperature for 24 h by covering the plate with thin foil. SDS is defined as MTT solvent that dissolves formazan crystals by producing a purple solution. At the end of the incubation time, the absorbance of each well was measured at 620 nm using ELISA reader (Tecan Systems Inc., San Jose, CA, USA).

ATR-FTIR spectroscopy experiments

Sample preparation

In ATR-FTIR spectroscopy measurements, 2×10^6 BM-MSCs at passage 3 were used. MSC cells harvested by 5-min centrifugation at 1,500 rpm (Eppendorf International 5810) after 10-min trypsin (0.25 % trypsin+1 mM EDTA) treatment at 37 °C in a 5 % CO_2 environment. Then, cell pellet was washed twice with 1-ml 0.9 % PBS solution to remove all growing media. The cell pellet was re-suspended in 10-μl 0.9 % PBS buffer, and then cell suspension was deposited on Diamond/ZnSe (Di/ZnSe) crystal plate of the Universal ATR unit of the FTIR spectrometer by rapidly evaporating using mild N_2 flux for 30 min to obtain a homogenous film of the entire cells on ATR crystal.

Data acquisition and spectroscopic measurements

Infrared spectra were obtained by scanning the prepared homogenous BM-MSCs film on Di/ZnSe crystal plate of the Universal ATR of Spectrum 100 FTIR spectrometer in the one-bounce ATR mode (Perkin-Elmer Inc.,

Norwalk, CT, USA). The spectra of BM-MSCs were recorded in the 4,000–650 cm^{-1} region at room temperature. Each interferogram was collected with 100 scans at 4 cm^{-1} resolution. The spectrum of atmospheric water vapor and carbon dioxide interference were recorded as background and then subtracted automatically using the Spectrum One software program. In order to prevent inorganic phosphate contribution in PBS to the spectrum, 10 μl PBS buffer was first dried with nitrogen (N_2) flux at identical conditions with the sample and the buffer spectrum was subtracted from the cell spectra. Recording and analysis of the spectral data were performed using the Spectrum One software from Perkin Elmer. Before the spectral analysis is performed, according to the requirements of analysis technique, some preprocessing steps are applied to the spectral data sets to make the spectra comparable. By these preprocessing approaches, the number of variables can either be reduced to prevent overfitting. Baseline correction, which is mainly used to get rid of a sloping and curving baseline, is a wavelength-dependent intercept and unique for each sample spectrum. The detailed data analysis and accurate determination of the variations in band area, values original baseline corrected spectrum was considered, while the band positions (frequency values) were measured according to the center of weight of the peaks from raw spectral data. All these mentioned quantitative analysis were performed on non-normalized but preprocessed average spectra. However, by the purpose of visual presentation of the differences, the average spectra of sampling groups were normalized with respect to the specific bands.

Cluster analysis

Cluster analysis was applied to find out spectral variations among sampling groups that were investigated in the study. OPUS 5.5 software (Bruker Optic, GmbH) was used to obtain the first derivative and vector-normalized spectra of each BM-MSC belonging to different age groups. Then, the cluster analysis was applied to these spectra in order to distinguish samples according to their spectral similarities and differences. The result of the analysis is represented in the form a dendrogram. The change in variances between the spectra of samples is represented by heterogeneity values. Higher heterogeneity between the clusters demonstrates higher differences among analyzed groups. Pearson's correlation coefficients were used to measure the distances between the pairs of spectra. Ward's algorithm was used to construct dendrograms for hierarchical clustering. The details of the calculation and algorithm can be found in Severcan et al. (2010).

Statistical analysis

The results of spectral measurements and MTT proliferation assay were expressed as "mean±standard error" values. At first, the experimental data were evaluated by normality test to decide whether the parametric or non-parametric statistical test to be used. Since the data showed normal distribution, all the results were evaluated by using one-way ANOVA and Tukey's multiple comparison test by considering their statistical significances in terms of $*p<0.05$, $**p<0.01$, and $***p<0.001$.

FTIR microspectroscopy experiments

Slide preparation

Passage 3 BM-MSCs were trypsinized, and after the trypsin was blocked with 10 % FBS, cells were collected with centrifugation at 1,500 rpm (Eppendorf International 5810) for 5 min, washed with PBS once, and then the two final washings were performed with normal saline solution to remove salt crystals. The cell pellet was dissolved in 1 ml of culture medium, and BM-MSCs were counted with Thoma lam by using trypan blue. MSCs (25.000) were placed on silver (Ag/SnO_2)-coated low-e microscope slides, and they were grown on at 37 °C in a 5 % CO_2 environment by overnight cultivation. At the end of cultivation time, BM-MSCs on low-e microscope slide were fixed by 10 % formalin for 10 min. In order to remove excess formalin, slides were washed with serum physiologic solution, and then, they were kept in dry environment to evaporate excess solution at room temperature for at least 1 h.

Collection of spectral images and preprocessing of spectral data

Perkin Elmer FTIR microscope coupled with Perkin Elmer Spotlight 400 software was used to map BM-MSC samples on microscope slides. The microscope is equipped with a liquid nitrogen cooled MCT detector and a CCD camera to provide an optical image of the

area under interrogation. An aperture size of 6.25 μm × 6.25 μm was used to obtain spectra from confluent monolayers. IR image maps were collected in the reflection mode through the spectral range 4,000–700 cm^{-1} with a 4 cm^{-1} resolution and 32 scan numbers. Background spectra were collected from a separate piece of blank MirrIR low-e slide. ISys software (Spectral Dimensions, Olney, MD, USA) was used to analyze the conventional FTIR microspectroscopic data. Whole baseline correction was performed between 3,800 and 800 cm^{-1} region. Then spectral masking was applied for analysis by using ISys software to get rid of the contributions from the surface around the cellular regions by marking the cells. The chemical maps were constructed for each group by taking area of specifically selected spectral bands arisen from lipids, proteins, and nucleic acids.

Acknowledgments The study was supported by METU internal funds and also by Hacettepe University DPT 2006 K 120 640-06-PEDİ-STEM project fund. Thanks to Fatima Aerts Kaya for her support during flow cytometry analysis.

Conflict of interest The authors declare that no conflict of interest exists.

References

Aggarwal S, Pittenger MF (2005) Human mesenchymal stem cells modulate allogeneic immune cell responses. Blood 105: 1815–1822

Aksoy C, Guliyev A, Kaya E, Uckan D, Severcan F (2012) Bone marrow mesenchymal stem cells in patients with beta thalassemia major: molecular analyses with attenuated total reflection-Fourier transform infrared spectroscopy study as a novel method. Stem Cells Dev 21(11):2000–2011

Baksh D, Song L, Tuan RS (2004) Adult mesenchymal stem cells: characterization, differentiation, and application in cell and gene therapy. J Cell Mol Med 8(3):301–316

Baxter MA, Wynn RF, Jowitt SN et al (2004) Study of telomere length reveals rapid aging of human marrow stromal cells following in vitro expansion. Stem Cells 22:675–682

Bechtel HA, Martin MC, May TE, Lerch P (2009) Improved spatial resolution for reflection mode infrared microscopy. Rev Sci Instrum 80:126106

Cakmak G, Togan I, Severcan F (2006) 17β-Estradiol induced compositional, structural and functional changes in rainbow trout liver, revealed by FT-IR spectroscopy: a comparative study with nonylphenol. Aquat Toxicol 77:53–63

Cakmak G, Zorlu F, Severcan M, Severcan F (2011) Screening of protective effect of amifostine on radiation-induced structural and functional variations in rat liver microsomal membranes by FT-IR spectroscopy. Anal Chem 83:2438–2444

Cakmak G, Miller LM, Zorlu F, Severcan F (2012) Amifostine, a radioprotectant agent, protects rat brain tissue lipids against ionizing radiation induced damage: an FTIR microspectroscopic imaging study. Arch Biochem Biophys 520(2):67–73

Campisi J, Sedivy J (2009) How does proliferative homeostasis change with age? What causes it and how does it contribute to aging? J Gerontol A Biol Sci Med Sci 64(2):164–166

Conboy IM, Rando TA (2012) Heterochronic parabiosis for the study of the effects of aging on stem cells and their niches. Cell Cycle 11(12):2260–2267

Di Giambattista L, Pozzi D, Grimaldi P, Gaudenzi S, Morrone S, Castellano AC (2011) New marker of tumor cell death revealed by ATR-FTIR spectroscopy. Anal Bioanal Chem 399: 2771–2778

Dillin A, Hsu AL, Arantes-Oliveira N, Lehrer-Graiwer J, Hsin H, Fraser AG, Kamath RS, Ahringer J, Kenyon C (2002) Rates of behavior and aging specified by mitochondrial function during development. Science 298:2398–2401

Dogan A, Ergen K, Budak F, Severcan F (2007) Evaluation of disseminated candidiasis on an experimental animal model: a Fourier transform infrared study. Appl Spectrosc 61:199–203

Dominici M, Le Blanc K, Mueller I et al (2006) Minimal criteria for defining multipotent mesenchymal stromal cells. The International Society for Cellular Therapy position statement. Cytotherapy 8:315–317

Dovbeshko GI, Gridina NY, Kruglova EB, Pashchuk OP (2000) FTIR spectroscopy studies of nucleic acid damage. Talanta 53:233–246

Drummond-Barbosa D (2008) Stem cells, their niches and the systemic environment: an aging network. Genetics 180: 1787–1797

Dukor R (2002) In: Chalmers J (ed) Handbook of vibrational spectroscopy. Wiley, New York, pp 3335–3361

Erukhimovitch V, Talyshinsky M, Souprun Y, Huleihel M (2005) FTIR microscopy detection of cells infected with viruses. Methods Mol Biol 292:161–172

Gaigneaux A, Ruysschaert JM, Goormaghtigh E (2006) Cell discrimination by attenuated total reflection–Fourier transform infrared spectroscopy: the impact of preprocessing of spectra. Appl Spectrosc 60:1022–1028

Gorgulu ST, Doğan M, Severcan F (2007) The characterization and differentiation of higher plants by Fourier transform infrared spectroscopy. Appl Spectrosc 61:300–308

Haris PI, Severcan F (1999) FTIR spectroscopic characterization of protein structure in aqueous and non-aqueous media. J Mol Catal B Enzym 7(1–4):207–221

Harris DT (2012) Opinion: younger Is better. The Scientiest Web http://www.the-scientist.com/?articles.view/articleNo/32483/title/Opinion–Younger-Is-Better/

Huang K, Zhou DH, Huang SL, Liang SH (2005) Age-related biological characteristics of human mesenchymal stem cells from different age donors. J Exp Hematol 13(6):1049–1053

Ishii K, Kimura A, Kushibiki T et al (2007) Fourier transform infrared spectroscopic analysis of cell differentiation. Opt Tissue Eng Reg Med 6439: 64390I-1-7

Kazarian SG, Chan KL (2006) Applications of ATR-FTIR spectroscopic imaging to biomedical samples. Biochim Biophys Acta 1758:858–867

Kneipp J, Lasch P, Baldauf E et al (2000) Detection of pathological molecular alterations in scrapie-infected hamster brain by Fourier transform infrared (FT-IR) spectroscopy. Biochim Biophys Acta 1501:189–199

Kollman C, Howe CWS, Anasetti C, Antin JH, Davies SM et al (2001) Donor characteristics as risk factors in recipients after transplantation of bone marrow from unrelated donors: the effect of donor age. Blood 98:2043–2051

Krafft C, Salzer R, Seitz S et al (2007) Differentiation of individual human mesenchymal stem cells probed by FTIR microscopic imaging. Analyst 132:647–653

Kretlow JD, Jin YQ, Liu W (2008) Donor age and cell passage affects differentiation potential of murine bone marrow-derived stem cells. BMC Cell Biol 9:60

Lazarus HM, Koc ON, Devine SM, Curtin P et al (2005) Cotransplantation of HLA-identical sibling culture-expanded mesenchymal stem cells and hematopoietic stem cells in hematologic malignancy patients. Biol Blood Marrow Transplant 11:389–398

Leskovjan AC, Kretlow A, Miller LM (2010) Fourier transform infrared imaging showing reduced unsaturated lipid content in the hippocampus of a mouse model of Alzheimer's disease. Anal Chem 82:2711–2716

Manoharan R, Baraga JJ, Rava PR et al (1993) Biochemical analysis and mapping of atherosclerotic human artery using FT-IR microspectroscopy. Atherosclerosis 103:181–193

Mareschi K, Ferrero I, Rustichelli D, Aschero S et al (2006) Expansion of mesenchymal stem cells isolated from pediatric and adult donor bone marrow. J Cell Biochem 97:744–754

Matthaus C, Boydston-White S, Miljkovic M, Romeo MJ, Diem M (2006) Raman and infrared microspectral imaging of mitotic cells. Appl Spectrosc 60:1–8

Naumann D (2001) FT-infrared and FT-Raman spectroscopy in biomedical research. Appl Spectrosc Rev 36(2–3):239–298

Parker FS (1971) Application of infrared spectroscopy in biochemistry, biology and medicine. Plenum Press, New York

Peuchant E, Richard-Harston S, Bourdel-Marchasson I, Dartigues JF (2008) Infrared spectroscopy: a reagent-free method to distinguish Alzheimer's disease patients from normal-aging subjects. Transl Res 152:103–112

Pittenger MF, Mackay AM, Beck SC (1999) Multilineage potential of adult human mesenchymal stem cells. Science 284: 143–147

Raggi C, Berardi AC (2012) Mesenchymal stem cells, aging and regenerative medicine. Muscles Ligaments Tendons J 2(3): 239–242

Rando TA (2006) Stem cells, ageing and the quest for immortality. Nature 441:1080–1086

Rigas B, Morgello S, Goldman IS, Wong PTT (1990) Human colorectal cancers display abnormal Fourier transform infrared spectra. Proc Natl Acad Sci U S A 87(20):8140–8144

Severcan F, Kaptan N, Turan B (2003) Fourier transform infrared spectroscopic studies of diabetic rat heart crude membranes. Spectrosc Int J 17(2–3):569–577

Severcan F, Gorgulu G, Gorgulu ST, Guray T (2005) Rapid monitoring of diabetes induced lipid peroxidation by Fourier transform infrared spectroscopy: evidence from rat liver microsomal membranes. Anal Biochem 339:36–40

Severcan F, Bozkurt O, Gurbanov R, Gorgulu G (2010) FT-IR spectroscopy in diagnosis of diabetes in rat animal model. J Biophotonics 3:621–631

Signer RAJ, Morrison SJ (2013) Mechanisms that regulate stem cell aging and life span. Cell Stem Cell 12(2):152–165

Tabbara IA, Zimmerman K, Morgan C, Nahleh Z (2002) Allogeneic hematopoietic stem cell transplantation: complications and results. Arch Intern Med 162: 1558–1566

Tokalov SV, Grüner S, Schindler S (2007) Age-related changes in the frequency of mesenchymal stem cells in the bone marrow of rats. Stem Cells Dev 16:439–446

Tower J (2012) Stress and stem cells. Dev Biol 1:789–802

Van de Loosdrecht AA, Beelen RH, Ossenkoppele GJ (1994) A tetrazolium-based colorimetric MTT assay to quantitate human monocyte mediated cytotoxicity against leukemic cells from cell lines and patients with acute myeloid leukemia. J Immunol Methods 174:311–320

Wagner W, Horn P, Bork S, Ho AD (2008) Aging of hematopoietic stem cells is regulated by the stem cell niche. Exp Gerontol 43:974–980

Wagner W, Bork S, Lepperdinger G, Joussen (2010) How to track cellular aging of mesenchymal stromal cells? Aging 2:224–230

Wilson A, Shehadeh LA, Yu H, Webster KA (2010) Age-related molecular genetic changes of murine bone marrow mesenchymal stem cells. BMC Genomics 11:229

Zheng H, Martin J, Duwayri Y (2007) Impact of aging on rat bone marrow-derived stem cell chondrogenesis. J Gerontol A Biol Sci Med Sci 62:136–148